RAPORTUL ŞTIINŢIFIC ŞI TEHNIC (RST)

Programul: **Parteneriate in domenii prioritare**
Acronim proiect: **SYNBIOCAT**
Contract nr: **124/2012**

ETAPA 2015: Scale up of biocatalysts immobilization

Având în vedere faptul că rezultatele experimentale incluse în această etapă a proiectului au constituit subiectele unor lucrări publicate sau acceptate spre publicare în reviste cotate ISI, raportul va fi redactat în limba engleză, respectând informaţiile originale din articolele menţionate.

A. COMPARATIVE ANALYSIS OF LIPIDS BIOCONVERSION USING FREE AND IMMOBILIZED BIOCATALYSTS

1. GENERAL OBJECTIVES – PROJECT STAGE ABSTRACT

The researches included in this stage of the project have been focused on the kinetic, diffusional and mixing efficiency aspects of the lipids bioconversion using free and immobilized cells of *Bacillus spp.* and *Yarrowia lipolytica* cells.

The experiments have been directed to enzymatic and fermentative systems with important economic potential (biodegradation of lipids from different media belonging to food, pharmaceutical, and chemical industries), being carried out in two types of bioreactors: mechanically stirred and pneumatic ones.

The results have been analyzed comparatively to the classical systems, from the point of view of the used enzymes and microorganisms, as well as of the used bioreactors, underlining that the considered systems represent efficient alternatives.

2. COMPARATIVE STUDIES ON KINETICS OF ANAEROBIC AND AEROBIC BIO-DEGRADATION OF LIPIDS FROM OLIVE OIL MILL WASTEWATERS WITH MIXTURE OF *Bacillus spp.* CELLS

Lipids are organic water insoluble biomolecules produced in different amounts by microbial, vegetal, and animal cells. Among the complex lipids, a particular class includes the triglycerides, namely fats and oils.

Our studies are focused on the analysis of the performances of the anaerobic and aerobic biological treatments of olive oil mill wastewaters using mixed *Bacillus spp.* culture. By means of the experimental results, a new and more complex kinetic model for aerobic bacterial bioconversion of lipids has been proposed and compared with that from literature.

The experiments were carried out in 2 L laboratory stirred bioreactor (Fermac, Electrolab), provided with computer-controlled and recorded parameters. The bioreactor mixing system consists of one turbine impeller and three baffles. The bioreactor and impeller characteristics are given in Table 1.

Table 1. Characteristics of bioreactor and impeller.

d, mm	d/D	H/D	w/d	l/d	h/d	No. blades	No. baffles
55	0.46	1.46	0.27	0.31	0.64	6	3

For the anaerobic biodegradation process, the dissolved oxygen amount from medium was not controlled during the process, varying free from its initial value of 1.6 mg/L. For the aerobic process, the bioreactor was provided with the sparging system consisting of a perforated tube with 7 mm diameter, placed at 15 mm from the vessel bottom, having 4 holes with 1 mm diameter. The air volumetric flow rate was varied between 5 and 30 L/h, in order to maintain the dissolved oxygen concentration at a prescribed constant value in the domain of 1.6 - 5.9 mg/L. The rotation speed was

maintained at 150 rpm. The bioreactor contained 1 L of olive oil - water emulsion (the oil concentration was 10 mg/L emulsion). According to the previous studies on olive oil biodegradation with *Bacillus spp.* cells (Caşcaval, 2012), the pH and temperature have been adjusted and maintained at the optimum values, namely 8 and 40 ^{o}C, respectively.

In the experiments, mixture of *Bacillus spp.* has been used (*Bacillus subtilis, Bacillus megaterium, Bacillus licheniformis*, and *Bacillus ortoliquefaciens* in equal ratios). The concentration of bacteria cells was 1 g d.w./100 ml medium. The fermentation end has been considered when either the olive oil was completely consumed or its concentration remained constant for 12 h. The process evolution has been analyzed by means of the variation of total lipids, using the spectrophotometric method with triolein (Levy, 1972).

The variation of total lipids concentration from wastewater during the anaerobic and aerobic biodegradation process with free *Bacillus spp.* cells is plotted in Figure 1.

It can be observed that the concentration of lipids is more rapidly decreased in the aerobic process, the rate of lipids consumption being accelerated by increasing the concentration of oxygen in the medium. Therefore, for the anaerobic biodegradation, the total lipids content is reduced to 1.3 g/L after 60 h, while for aerobic process it is possible to become 0 g/L after 40 h, depending on the oxygen concentration.

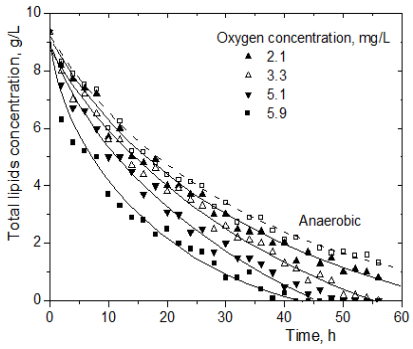

Figure 1. Variation of total lipids concentration during their anaerobic and aerobic bacterial biodegradation.

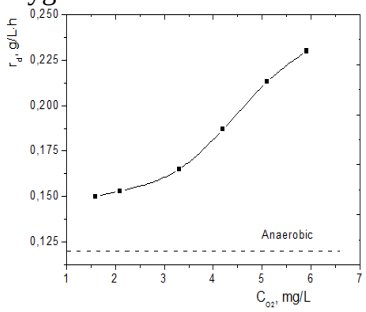

Figure 2. Influence of oxygen concentration on average rate of lipids bacterial biodegradation.

These results can be suggestively underlined by plotting in Figure 2 the dependence between the average rate of lipids biodegradation and the value of dissolved oxygen concentration. The average rate of process is defined by the following relationship:

$$\bar{r}_d = \frac{C_{TL0} - C_{TL}}{t} \qquad (1)$$

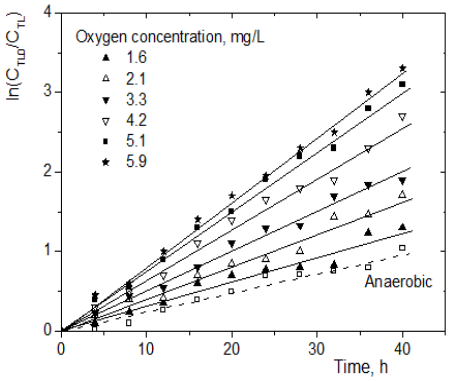

Figure 3. Graphical calculation of specific biodegradation rate (for anaerobic process) and apparent specific biodegradation rate (for aerobic process).

Because the oxygen concentration inside the medium is controlled and maintained at a constant level during the aerobic biodegradation process, the value of k_d' could be calculated at different oxygen concentrations similarly to the above presented algorithm, by plotting the corresponding straight lines (Figure 3).

The values of specific rate and modified specific rates at different concentrations of oxygen in medium are given in Table 2.

Table 2. Values of specific rate, k_d, and modified specific rate, k_d', of lipids biodegradation with cells of *Bacillus spp.*

C_{O2}, mg/L	Anaerobic	1.6	2.1	3.3	4.2	5.1	5.9
k_d, k_d' x 10^2, h^{-1}	2.61	3.53	3.7	4.76	6.4	7.55	8.12

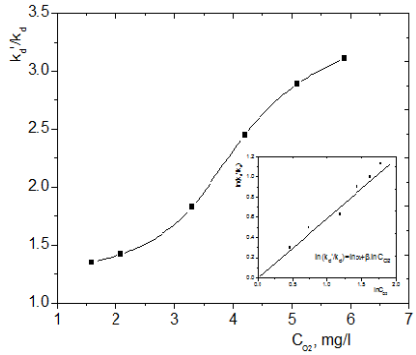

Figure 4. Influence of oxygen concentration on ratio k_d'/k_d.

For quantifying the influence of aerobic conditions on the rate of lipids biodegradation with *Bacillus spp.*, it was analyzed the variation of the ratio k_d'/k_d with the increase of oxygen concentration. This dependence, plotted in Figure 4, suggests the following exponential correlation:

$$\frac{k_d'}{k_d} = \alpha \cdot C_{O2}^{\beta} \qquad (2)$$

The values of coefficient α and exponent β can be calculated graphically by liniarizing the equation (2), according to Figure 4. Therefore, equation (2) becomes:

$$\frac{k_d'}{k_d} = C_{O2}^{0.62} \qquad (3)$$

Consequently, the aerobic degradation of lipids from olive oil using *Bacillus spp.* can be described by the following kinetic model:

$$-\frac{dC_{TL}}{dt} = k_d \cdot C_{O2}^{0.62} \cdot C_{TL} \qquad (4)$$

In conclusion, although the dissolved oxygen concentration in the medium exhibits an important influence on efficiency of biodegradation of lipids, the kinetic model proposed in literature does not include any term related to the oxygen concentration. Consequently, by means of the correlation between the modified specific rate, which includes the influence of oxygen concentration, specific rate, for the anaerobic biodegradation, and oxygen concentration, it was established a new kinetic model adequate for aerobic process. This model offers a good concordance with the experimental results, the average deviation of the calculated values of lipids biodegradable rate from the experimental ones being ± 6.84%.

NOTATIONS

C_{O2}	dissolved oxygen concentration, mg/L
C_{TL}	total lipids concentration in wastewater, g/L
C_{TL0}	initial total lipids concentration in wastewater, g/L
k_d	specific rate of lipids biodegradation process, h^{-1}
k_d'	modified specific rate of lipids biodegradation process considering the dissolved oxygen concentration, h^{-1}
t	time, h

3. COMPARATIVE ANALYSIS OF MIXING EFFICIENCY AND DISTRIBUTION IN A SPLIT-CYLINDER GAS-LIFT BIOREACTOR CONTAINING FREE AND IMMOBILIZED *Yarrowia lipolytica* CELLS

These experiments have been dedicated to the comparative analysis of mixing in a pneumatic bioreactor of split-cylinder gas-lift type (Figure 5) with free and immobilized cells of *Y. lipolytica*, for the process of lipids bioconversion.

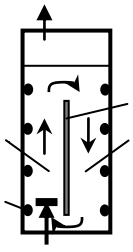

Figure 5. Schematic diagram of the experimental split-cylinder gas-lift bioreactor
(1 - riser, 2 - downcomer, 3 - baffle, 4 - point on mixing time measurement).

3.1. Distribution of mixing efficiency in a split-cylinder gas-lift bioreactor for free *Yarrowia lipolytica* cells suspensions

Pneumatic bioreactors are used at large-scale for the biotechnological production of chemicals or pollutants treatment. These bioreactors generate the broth circulation by means of the difference on hydrostatic pressure or density from different regions inside the broth. *Yarrowia lipolytica*, also named *Candida lipolytica*, is an ascomycetous yeast possessing the ability to convert various substrates (alkanes, lipids, sugars and derivatives, fatty by-products or wastewaters containing lipids, lignocellulosic residues, etc.) for accumulating inside the cells specific lipids (i.e., enriched in essential polyunsaturated fatty acids),

oils used in biodiesel synthesis, as well as lipolytic enzymes and other bioproducts (citric acid, ethanol, etc.). Although *Y. lipolytica* strains have been cultivated in various conditions and bioreactors types (stirred or gas-lift bioreactors, in batch, fed-batch or continuous regime), the engineering aspects, namely effects of operating conditions on broths hydrodynamics, rates of mass and heat transfers, cells physical integrity, etc. have to be elucidated for scaling-up these processes.

The aim of our studies is to establish the distribution of mixing efficiency inside the split-cylinder gas-lift bioreactor, by means of the mixing time values recorded at various positions of pH electrode, as well as the influences of biomass concentration and bioreactor operating parameters on the interchange of active and stagnant regions positions. For underlining the effects of the biomass presence on mixing efficiency, the experiments have been previously carried out for viscous simulated broths without biomass. This study has been focused on the investigation of mixing intensity and its distribution for *Y. lipolytica* suspensions. By means of the experimental data, mathematical correlations between the mixing time and the considered parameters have been established both for the riser and downcomer zones.

The experiments have been carried out in 6 l (5 l working volume) laboratory split-cylinder gas-lift bioreactor FerMac 310/60 (Electrolab), with computer-controlled and recorded parameters (Figure 5). The bioreactor reactor consists of a glass cylinder with 0.49 m height and 0.125 m diameter. For dividing the flow into the riser and downcomer regions with similar cross areas, a rectangular stainless steel baffle having 0.285 m height, 0.125 m width, and $2x10^{-3}$ m thickness was diametrically inserted into the glass column. The baffle was located at a distance of 0.04 m from the bottom of the reactor.

The air sparger consists of a perforated tube with $5x10^{-3}$ m diameter and 0.05 m length, being placed at 0.08 m from the bottom of the bioreactor. In order to avoid the slugging effect, air flow rate varied between 20 and 100 l/h, which correspond to a superficial velocity of 0.45 - $2.25x10^{-3}$ m/s. In the experiments, *Y. lipolytica* suspensions with cells concentration varying between 10 and 50 g/l d.w. have been used. These yeast concentrations correspond to suspension apparent viscosity domain of 2.7 - 9.5 cP. Owing to the difficulty of *in-situ* measurement of viscosity during the experiments, the viscosity was measured before and after each experiment using a viscometer of Viscotester 6 Plus type (Haake). Both the experiments and viscosity measurements were carried out at a temperature of 30^{o}C. Any viscosity or cells morphology change were recorded during the experiments.

The mixing efficiency has been analyzed by means of the mixing time values, measuring the pH variation for a tracer volume of 0.5 ml. The tracer was injected in the riser region, at 0.05 m from the bioreactor central axis and 0.38 m from the liquid surface. Because the tracer solution density is close to that of liquid phase, the tracer solution flow follows the liquid flow streams without errors due to the tracer buoyancy. The pH electrode (Mettler Toledo) was introduced initially in the riser region, then in the downcomer one. In both cases, it was placed at four different positions on the liquid height, varying from bioreactor bottom as follows (Figure 5): position 1: at 0.06 m; position 2: at 0.16 m; position 3: at 0.26 m; position 4: at 0.36 m.

The mathematical correlations, which describe separately the influences of considered factors on mixing time for *Y. lipolytica* suspensions at various positions inside the riser and downcomer regions have been developed using MATLAB software. For the experimental data, a multiregression analysis was performed, the difference between the experimental and modeled value being reduced to a minimum by least-square fit method. By means of a MATLAB program, the regression coefficients and standard deviations were calculated.

During the fermentation process, the appearance and extending of the stagnant regions in the bioreactor cannot be avoided, due to the continuous modification of the rheological characteristics or behavior of the broths. Regardless of the bioreactor type, the aerated broths flow is more complex compared to that of non-aerated broths, due to the contribution of pneumatic agitation on fluid circulation pattern.

The heterogeneity and, implicitly, complexity of the broth hydrodynamics are more pronounced in the case of internal-loop gas-lift bioreactors, due to the cyclic pattern of fluid flow. In this case, besides the rheological properties of the biomass suspensions, concentration and deposition tendency of cells, the efficiency and distribution of mixing are controlled by a lot of geometrical and operational characteristics of the bioreactor: height, riser and downcomer cross areas ratio, height of gas separation and clearance regions, gas input rate. The riser region is associated with the largest velocity of liquid phase, generating the most intense mixing, and allows to reaching the highest rate of mass and heat transfer, as well as the most important shear stress. Although to the previous studies on viscous media without biomass indicated that the variation of mixing efficiency on the riser height is directly controlled by the value of gas input rate and fluid phase viscosity, the presence of biomass could generate the change both of the mixing intensity and of its distribution along the riser region.

Thus, unlike the variation of mixing time recorded for simulated broths, Figure 6 indicates that the increase of aeration rate leads to the continuous intensification of mixing only for the positions 2, 3, and 4. For position 1, placed at the bottom of the riser, the value of mixing time decreases by intensifying the aeration, reaches a minimum level, then increasing. The value of aeration rate corresponding to the minimum of mixing time is reduced from 1.35 $x10^{-3}$ to 1.05$x10^{-3}$ m/s by *Y. lipolytica* cells accumulation. Moreover, for the entire considered ranges of air superficial velocity and biomass concentration, the less intense mixing was recorded for this region.

The particular variation of mixing intensity related to the position 1 is the result of two phenomena induced by yeast cells accumulation. On the one hand, due to the biomass deposition, the interactions of friction type between the yeast cells are higher compared to the superior positions, this leading to the reduction of suspension upward circulation velocity. Moreover, due to the buoyancy tendency of the bubbles entrapped in the descending flow, the suspension circulation velocity in the downcomer region is lowered.

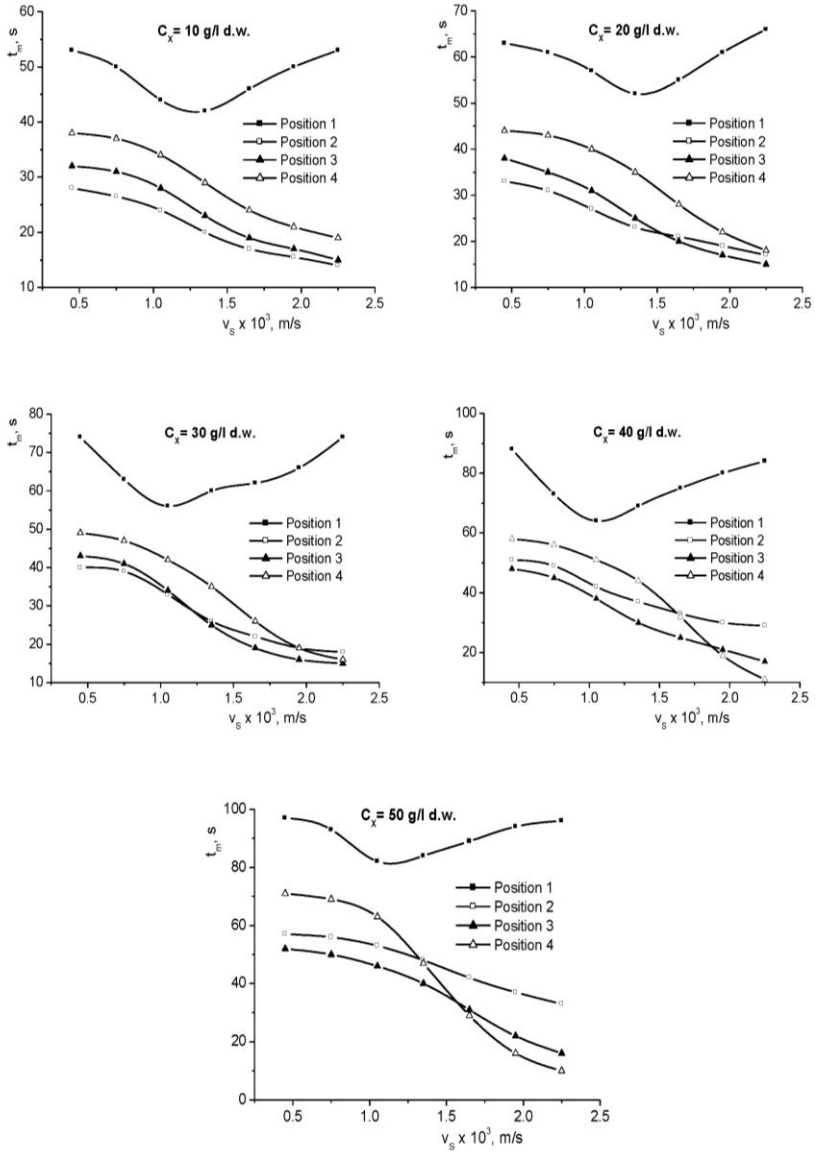

Figure 6. Influence of air superficial velocity on mixing time for *Y. lipolytica* cells suspensions at different pH electrode positions in the riser.

The magnitude of this effect is amplified by intensifying the aeration and at higher *Y. lipolytica* cells concentration, due to the increased viscosity of suspension and to the deposition of solid phase which hinders the ascending circulation of the bubbles and promotes their stratification. Because the turbulence in inferior region of the riser is influenced mainly by the fluid circulation velocity in the clearance zone from the bioreactor bottom, the aforementioned phenomena control the mixing intensity in the region corresponding to position 1 of the downcomer.

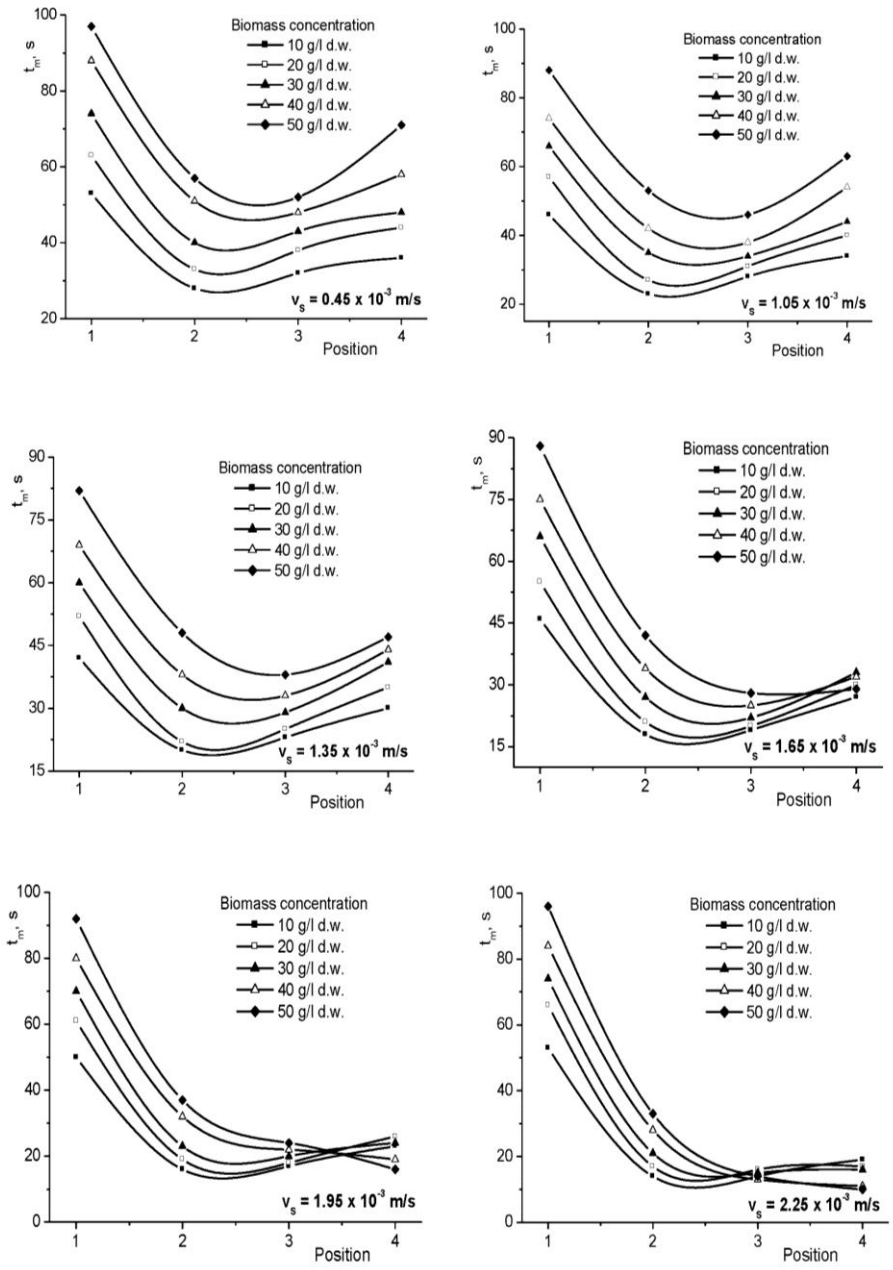

Figure 7. Variation mixing time on liquid height in the riser for *Y. lipolytica* cells suspensions at different air superficial velocities.

The magnitude of the positive effect of air superficial velocity on mixing efficiency recorded for the other three positions considered on the ascending flow of the suspension depends on the position and yeast concentration. Thus, at *Y. lipolytica* cells concentration up to 20 g/l d.w., the analysis of the variation of mixing time on riser height indicated that its highest values are reached for the top position, namely position 4 (Figure 8). The intermediary positions are placed closer to the sparger and correspond to the regions with the most intense turbulence. By increasing the yeast cells amount in the suspension and air input rate, the values of mixing time recorded for position 4 becomes near to those related to positions 2 and 3, being lowered for biomass concentration over 40 g/l d.w. and air superficial velocity higher than 1.65×10^{-3} m/s.

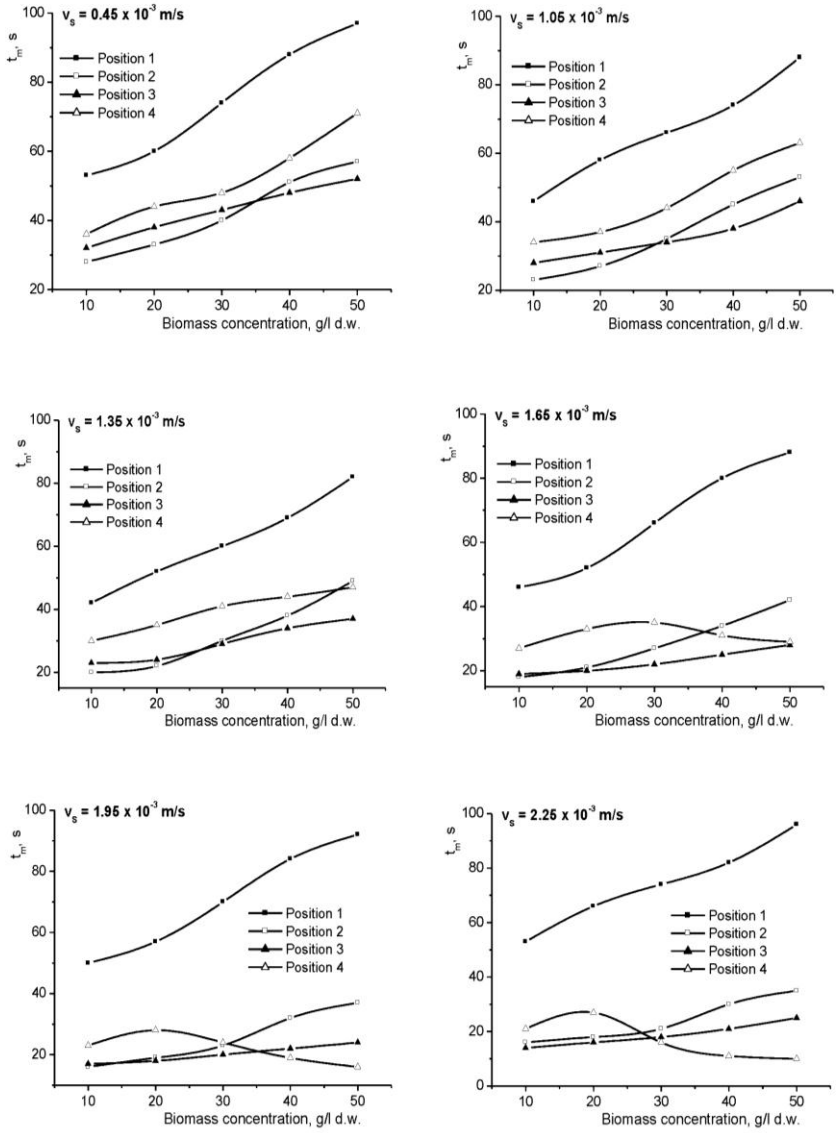

Figure 8. Influence of *Y. lipolytica* cells concentration on mixing time for different air superficial velocities and pH electrode positions in the riser.

The less important effect of increasing aeration rate on intensifying the mixing was recorded for position 2 (Figures 7 and 8). Consequently, at *Y. lipolytica* cells concentration of 50 g/l d.w., this region can be associated with the poorest mixing compared to positions 3 and 4.

The variation of the relative mixing intensity for these three positions is the result of the effects of biomass deposition and bubbles coalescence on bubble rising velocity and, implicitly, on turbulence extent. The process of bubbles coalescence occurs in cells suspensions or viscous media and becomes more important by increasing the air input rate and by cells accumulation. Therefore, for concentrated suspensions of *Y. lipolytica* cells, at higher aeration rate, it was observed the significant bubbles coalescence, this phenomenon leading to the heterogeneous distribution of air in the broth and acceleration of bubbles rising velocity through central route. Consequently, the mixing time is reduced due to the intensification of turbulence from position 2 to 4. The importance of this effect is enhanced by cells deposition to the riser bottom, due to the amplification of friction between the cells, which hinders the suspension circulation.

The variation of mixing time along the riser height for *Y. lipolytica* suspensions differs from that previously observed for simulated broths without biomass. As it was above concluded for yeast suspensions, the broth flow velocities in the regions of bottom clearance and top gas separation, namely positions 1 and 4, are controlled mainly by cells concentration in these regions, and less by flow section area as in the case of simulated viscous media.

The discussed effects are underlined by the dependence between the mixing time and the concentration of cells, plotted in Figure 9. Excepting the top position 4, the mixing time is continuously

increased by accumulation of *Y. lipolytica* cells, the most important influence being observed for the bottom region of the riser.

Similar variation has been recorded also for position 4, but only for air superficial velocities up to $1.35x10^{-3}$ m/s. In this case, the intensification of aeration promotes the dispersion of biomass also in the superior region of the riser, this phenomenon leading to the reduction of turbulence in this region. The intensification of aeration promotes the bubbles coalescence, with the above discussed positive consequences on the mixing time. Because the relative importance of these two contrary effects is controlled by yeast concentration in the suspension, for *Y. lipolytica* concentrations higher than 20 - 30 g/l d.w. and air superficial velocities over $1.35x10^{-3}$ m/s, the relative magnitude of the positive effect induced by acceleration of the rising velocity of larger bubbles generated by coalescence exceeds that of the negative effect of intensification of friction between cells by increasing the biomass concentration in the top position. In these circumstances, the suspension circulation velocity is accelerated at the top of the riser region and the value of mixing time decreases and becomes lower than those corresponding to the intermediary positions 2 and 3. For the same reasons, the mixing becomes more efficient in position 3 compared to position 2 at higher aeration rate and biomass concentration.

The experimental data have been included in some mathematical correlations which describe separately for the riser and downcomer regions the influence of *Y. lipolytica* cells concentration, superficial air velocity, and position on the bioreactor height on mixing time. Because of particular variation of mixing time for positions 1 of the riser and downcomer, one specific equation has been proposed for these two bottom regions.

The influences of the considered parameters on mixing efficiency for the other positions have been included in two distinct equations for the ascending and descending flows, respectively. The general expression of the proposed equations is:

$$t_m = \alpha \cdot C_X^{\beta} \cdot v_S^{\gamma} \cdot h^{\delta} \tag{5}$$

The influence and the relative importance of the considered variables are suggested by the coefficients α, β, γ, and δ values. The values of these coefficients are specific for each circulation region created by the split device inside the air-lift bioreactor, being calculated by the multiregression method using MATLAB software. Thus, the following correlations have been established:

- ***riser and downcomer, position 1***

$$t_m = 11.301 \cdot \frac{C_X^{0.496}}{v_S^{0.021\exp(h)}} \text{ , s} \tag{6}$$

- ***riser region, positions 2 - 4***

$$t_m = 0.226 \cdot \frac{C_X^{0.298} \cdot h^{0.089}}{v_S^{0.609}} \text{ , s} \tag{7}$$

- ***downcomer region, positions 2 - 4***

$$t_m = 7.494 \cdot \frac{C_X^{0.665}}{v_S^{0.011\ln h}} \text{ , s} \tag{8}$$

The proposed models are in concordance with the experimental data, the maximum deviation being of 8.82% for position 1, 7.42% for the riser, and 8.38% for the downcomer one. Analyzing the corresponding determination coefficients, which represent the square of correlation coefficients for the proposed equations, it can be concluded that the considered factors influence the mixing efficiency and distribution in an average extent of 94.6%. The rest of 5.4% can be attributed to the effects of other factors, namely: sparger position, ratio of cross areas of riser and downcomer flow regions, height of gas separation or bottom clearance regions, etc.

*

The studies on mixing intensity and distribution for *Y. lipolytica* suspensions in a split-cylinder gas-lift bioreactor revealed the different behaviors of broth flows in the riser and downcomer regions, especially from the point of view of variation of turbulence along the two regions height.

Therefore, the most intense mixing in the riser has been reached for the intermediary and top positions. Generally, the increase the yeast cells amount exhibited a negative effect on mixing efficiency. However, for the top position, the mixing time decreased for yeast concentration over than 20 - 30 g/l d.w. and air superficial velocity higher than $1.35x10^{-3}$ m/s, due to the more important positive effect on mixing

induced by the acceleration of the rising velocity of larger bubbles generated by coalescence than the negative effect of the intensification of friction between cells induced by increasing the biomass amount in this position.

The distribution of mixing intensity in the downcomer zone is rather similar, the highest turbulence being induced in the positions corresponding to the bottom and top of the descending stream, especially for concentrated suspensions and intense aeration (biomass concentration over 30 g/l d.w., air superficial velocity over 1.35×10^{-3} m/s). The positive influence of aeration rate on turbulence extent was recorded only for air superficial velocity up to 1.35×10^{-3}m/s. For higher values of air input rate and *Y. lipolytica* cells concentration, the phenomenon of bubbles entrapping in the downward flow became significant, this leading to the hindrance of broth circulation and, implicitly, to the increase of mixing time.

The influences of the considered factors on mixing intensity have been included in three mathematical correlations established separately for the riser and downcomer regions. The proposed equations allow to predicting the mixing time on the height of the internal-loop gas-lift for these two circulation regions of bioreactor and offer a good agreement with the experimental results.

NOTATIONS

C_X - yeast cells concentration, g/l d.w

h - distance from the bioreactor bottom, m

pH_∞ - pH-value corresponding to the perfect mixing

ΔpH - pH-limits accepted for mixing time determination

t_m - mixing time, s

v_S - air superficial velocity, m/s

α, β, γ, δ - parameters of equation (2)

3.2. Distribution of mixing efficiency in a split-cylinder gas-lift bioreactor for immobilized *Yarrowia lipolytica* cells suspensions

In these experiments, suspensions of alginate particles containing immobilized *Y. lipolytica* cells have been used. The immobilization was carried out by cells inclusion into the alginate matrix, according to the method given in literature (Williams and Munnecke, 1981). In this purpose, 10 g d.w. yeast cells were mixed with 100 ml of 5% aqueous solution of sodium alginate. The biocatalysts particles have been obtained by dripping this suspension at constant pressure through a capillary into a solution of 0.2% $CaCl_2$. Capillaries with three different diameters have been used and the obtained particles of immobilized cells had the following diameters: 3.0, 3.6 and 4.2 mm.

The volumetric fraction of the biocatalyst particles into the medium was 0.10.

The mixing efficiency has been also analyzed by means of the mixing time values. Each experiment has been carried out for three or four times, for identical conditions, the average value of mixing time being used. The maximum experimental errors were between 5.85 and 7.35%.

The analysis of the effect of aeration rate on mixing time for the riser, plotted in Figure 9, indicates the gradual change of the shapes of the curves describing this influence from the bioreactor bottom to its superior region. Moreover, the magnitude of the aeration rate influence depends also on the alginate particles size.

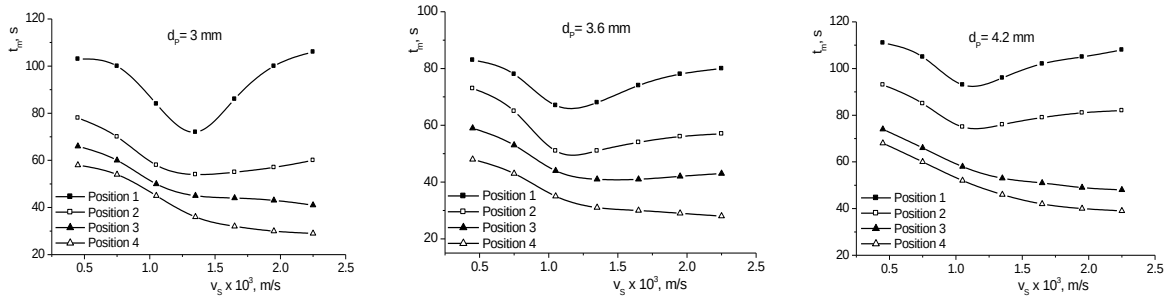

Figure 9. Influence of air superficial velocity on mixing time for immobilized *Y. lipolytica* cells suspensions at different pH electrode positions in the riser.

Regardless of the biocatalyst size, for the two positions placed at the bottom of the riser, namely positions 1 and 2, the value of mixing time decreases by intensifying the aeration, reaches a minimum level, increasing then. This variation is more obvious for position 1. The value of aeration rate corresponding to the minimum of mixing time is reduced from 1.35×10^{-3} to 1.05×10^{-3} m/s by increasing the size of the biocatalyst

particles. These two inferior positions are associated with the less intense mixing, for the entire considered ranges of air superficial velocity and particles size.

The particular variation of mixing intensity related to the positions 1 and 2 is the result of two phenomena induced by deposition of the biocatalyst particles. On the one hand, due to the solid phase accumulation at the riser bottom, the interactions of friction type between the particles are higher compared to those related to the superior positions, this leading to the reduction of suspension upward circulation velocity. Moreover, due to the buoyancy tendency of the bubbles entrapped in the descending flow, the suspension circulation velocity in the downcomer region is lowered (Merchuk and Gluz, 1999). The magnitude of this effect is amplified by intensifying the aeration and at higher alginate particles size, which possess higher deposition velocity and hinder the ascending circulation of the bubbles in the downcomer region, inducing their stratification. Because the turbulence in inferior region of the riser is controlled mainly by the fluid circulation velocity in the clearance zone from the bioreactor bottom, the aforementioned phenomena control the mixing intensity in the region corresponding to positions 1 and 2 of the riser.

Although the recorded variation of mixing time is similar for all the three experimented sizes of biocatalyst, from Figure 9 it can be observed that the lowest mixing time values for positions 1 and 2 are reached for the alginate particles having the intermediary diameter of 3.6 mm. Generally, the hindrance of suspension circulation is controlled both by the deposition of solid phase and by the supplementary friction forces induced by the interactions between the particles or between the particles and the bioreactors internal devices. Consequently, the effect of particles size on mixing time could be the result of the concurrence between the relative importance of the particles interactions, which create friction forces, and particles deposition to the bioreactor bottom, both phenomena inducing additional resistances to the suspension circulation. At the same volumetric fraction, the immobilized cells with 3 mm diameter possess an increased interfacial area with 20%, and, respectively, 40% than the particles with diameters of 3.6 and 4.2 mm. Therefore, for the smallest particles of biocatalyst, the contribution of the friction forces between the particles themselves or between the particles and the continuous phase is greater than that of the larger particles and exceeds the relative importance of the deposition process. On the other hand, the deposition velocity being direct proportional to the particle size, the deposition tendency of the biocatalyst particles with diameter of 4.2 mm is superior to those of the other two size particles and its relative importance exceeds that of the interactions between the particles. For this reason, the values of mixing time recorded for the positions 3 and 4 are closer for the largest particles compared to the smaller ones.

Figure 9 suggests that the deposition of the immobilized yeast cells generally exhibits a more important effect on these suspensions circulation velocity, because the highest values of mixing times have been recorded for biocatalyst particles with 4.2 mm diameter.

Because the use of the immobilized *Y. lipolytica* cells of 3.6 mm diameter balances the above discussed two negative phenomena, the most efficient mixing is reached for this size of biocatalyst particles.

For the superior positions 3 and 4, the intensification of aeration rate leads to the improvement of mixing, effect that is more important mainly for the smallest and largest biocatalyst particles (Figure 9). This variation is the result of the lower content of solid phase in the superior region of the riser compared to the inferior one, this diminishing the influence of friction and deposition processes on the medium flow.

The dependence between the mixing time and air superficial velocity for the intermediary size of biocatalyst particles in the superior region of the riser is rather different from those corresponding to the other two sizes, being similar to the variations recorded for the positions 1 and 2. In this case, as the result of the most intense mixing related to the particles of 3.6 mm diameter, the solid phase distribution on the riser height is more uniform, the particles content in the superior region of riser and, implicitly, in the downcomer is higher than for the other sizes of biocatalysts, and the effects observed for the positions 1 and 2 become more pronounced. However, for the positions 3 and 4, the most efficient mixing was recorded also for the alginate particles having the intermediary diameter.

Considering the values of mixing time, the mixing efficiency of immobilized *Y. lipolytica* suspensions is superior to that of the free cells suspensions, especially for the top positions on the riser (Caşcaval et al., 2015). The similar shapes of the mixing time variations related to the entire ascendent region height suggest a more uniform distribution of mixing for the biocatalyst particles suspensions compared to the *Y. lipolytica* free cells suspensions. In the same time, due to the significant larger size and different behavior of biocatalyst particles compared to the yeast cells, the bubbles coalescence has not been observed in this bioreactor as it has occurred in the *Y. lipolytica* free cells suspensions.

The variation of mixing time along the riser height for *Y. lipolytica* immobilized cells suspensions differs from that previously observed for simulated broths and free biomass cultures. As it was concluded for free *Y. lipolytica* cells suspensions, the suspensions flow velocities in the regions of bottom clearance and top

gas separation, namely positions 1 and 4, are controlled mainly by cells concentration in these regions, and less by flow section area, as in the case of simulated viscous media (Galaction et al., 2014; Caşcaval et al., 2015). For the alginate particles suspensions, Figure 10 indicates that the mixing time generally decreases from the bottom to the top region of the riser. This variation is the result mainly of the decrease of the solid phase amount on the riser height, due to its deposition. However, the relative magnitude of the mixing time reduction along the ascending flow region depends on the biocatalyst size and air superficial velocity.

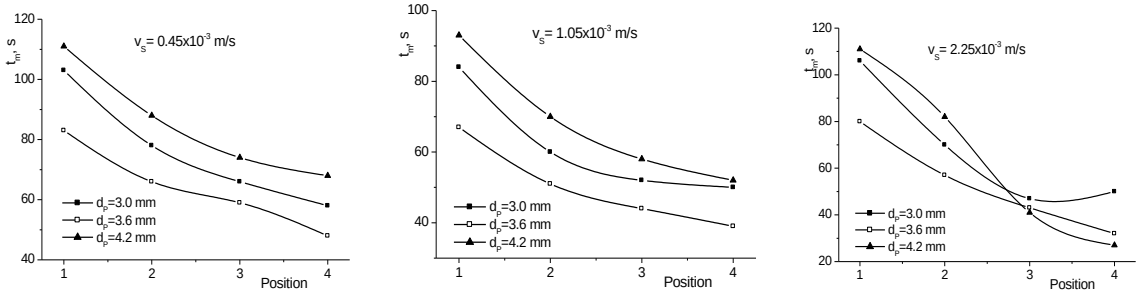

Figure 10. Variation mixing time on liquid height in the riser for immobilized *Y. lipolytica* cells suspensions at different air superficial velocities.

At low aeration rate, below 1.05x10^{-3} m/s, the mixing efficiency is continuously improved by increasing the distance from the bioreactor bottom for all the experimented sizes of the biocatalyst. In this case, regardless of the pH electrode position, the most efficient mixing is recorded for the alginate particles having the intermediary diameter, due to the above presented effects, while the less efficient one corresponds to the largest particles, as the consequence of the hindrance of liquid phase flow by their opposite circulation towards the riser bottom. By intensifying the aeration, this order of mixing time variation is respected only in the first half of the ascending flow region. For the superior region, the mixing time related to the smallest biocatalyst particles reaches a minimum value corresponding to position 3, then being gradually increased by increasing the air superficial velocity and exceeding those recorded for the other two sizes of biocatalyst for v_S over 1.05x10^{-3} m/s (Figure 10). This modification of the variation of mixing time along the riser height for the alginate particles with 3 mm diameter is due to the intensification of aeration which promotes the dispersion of solid phase also in the superior region of the riser, this phenomenon leading to the reduction of turbulence in this region.

Contrary, due to their more pronounced tendency of deposition, and, consequently, to their lower concentration in the positions 3 and 4, the mixing time recorded in the superior half of the riser for the largest biocatalyst particles becomes lower than that for the smallest ones at air superficial velocity over 1.05x10^{-3} m/s. Moreover, at higher aeration rate, the mixing time for 4.2 mm diameter alginate particles is inferior also to that corresponding to the intermediary size biocatalysts.

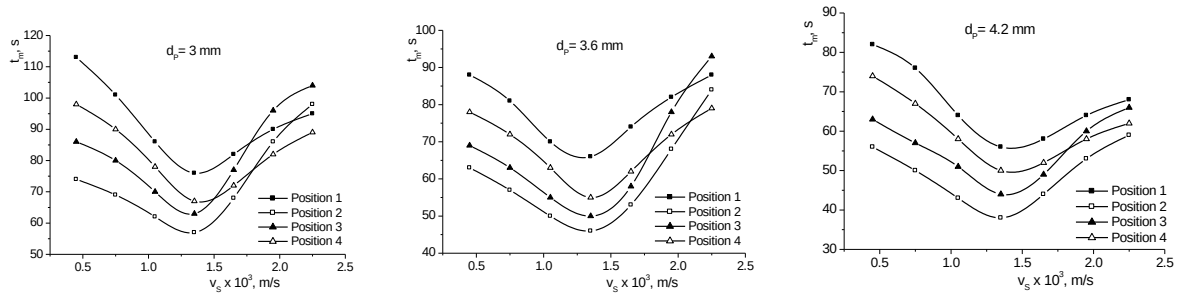

Figure 11. Influence of air superficial velocity on mixing time for immobilized *Y. lipolytica* cells suspensions at different pH electrode positions in the downcomer.

The suspension hydrodynamics in the downcomer is more complex, being controlled by the number and behavior of bubbles entrapped into the fluid which descends from the top to the bottom of this region. Obviously, in the case of this gas-lift bioreactor having similar riser and downcomer cross section areas, for all considered positions, Figure 11 indicates that the suspension velocity in the downcomer region is lower than that corresponding to the riser. Moreover, for all considered sizes of biocatalyst particles and contrary to the variations plotted in Figure 9 for the positions 2 to 4 on the riser.For aeration rate below 1.35x10^{-3} m/s, the highest values of mixing time were recorded for the bottom and top regions, namely positions 1 and 4, because the suspension flow velocities in the regions of bottom clearance and top gas separation are lower than those corresponding to the intermediary positions (Li et al., 2009). Owing to the solid phase deposition

and, implicitly, its higher amount at the bioreactor bottom, the mixing efficiency is inferior in position 1 compared to position 4.

For the air superficial velocity over $1.35x10^{-3}$ m/s, the most important reduction of turbulence was observed for positions 2 and 3, the mixing times corresponding to these positions exceeding those recorded for positions 4 and 1, respectively. This effect is attenuated by increasing the biocatalyst particles size.

According to the previous results, this behavior is the main consequence of the change of the relative importance of bubbles disengagement in the gas separation region and their entrapping into the suspension which circulates downward (Chisti and Moo-Young, 1988; Merchuk and Gluz, 1999; Caşcaval et al., 2015). Thus, at low air superficial velocity, the suspension flow velocity in the riser is low and allows separating completely the bubbles at the top of gas-lift bioreactor. As it was above discussed, the dispersion flow velocity in the riser increases by intensifying the aeration and leads to the entrapment of bubbles in the downward stream. Due to the buoyancy tendency of the bubbles, as well as to their accumulation, stratification, followed by their coalescence, the descending velocity of the dispersion is reduced and, implicitly, the mixing efficiency is affected. The presence and increase of the amount of *Y. lipolytica* immobilized cells in the downcomer exhibit a more significant effect on inducing the bubbles stratification compared to that observed for simulated broths without biomass or for free yeast cells suspensions (Galaction et al., 2014; Caşcaval et al., 2015). In the same time, the descending movement of solid phase, more important for the biocatalyst particles than for the biomass, hinders the ascending flow of the bubbles, reducing supplementary the suspension flow velocity. These phenomena are more important for the regions farther from the top or bottom of downcomer and are amplified for the smallest particles, due to their increased resistance against the ascending movement of the entrapped bubbles.

Although at higher aeration rate, the descending bubbles could reach the bottom zone of the gas-lift bioreactor and could be recirculated by the rising stream, inducing the increase of the turbulence in this region (Chisti and Moo-Young, 1988; Merchuk and Gluz, 1999), this effect was not observed in the given experimental conditions, which have been selected for avoiding the significant increase of air input rate, slug flow in the riser or the biocatalysts and cells mechanical lysis.

The experimental data have been included in two mathematical correlations which describe, separately for the riser and downcomer regions, the influences on mixing time of the size of immobilized *Y. lipolytica* particles, superficial air velocity, and position on the bioreactor height. The general expression of the proposed equations is:

$$t_m = \alpha \cdot C_X^{\beta} \cdot v_S^{\gamma} \cdot h^{\delta} \tag{9}$$

The influence and the relative importance of the considered variables are suggested by the coefficients α, β, γ, and δ values. The values of these coefficients are specific for each circulation region created by the split device inside the gas-lift bioreactor, being calculated by the multiregression method using MATLAB software. Thus, the following correlations have been established:

- ***riser region:***

$$t_m = 56.57 \cdot \frac{d_P^{0.517}}{v_S^{0.314} \cdot h^{0.434}}, \text{ s} \tag{10}$$

- ***downcomer region:***

$$t_m = 43.19 \cdot \frac{d_P^{0.655}}{v_S^{0.418\exp(h)}}, \text{ s} \tag{11}$$

The proposed models are in concordance with the experimental data, the maximum deviation being of 7.62% for the riser and 8.30% for the downcomer. Analyzing the corresponding determination coefficients, which represent the square of correlation coefficients for the proposed equations, it can be concluded that the considered factors influence the mixing efficiency and distribution in an average extent of 93.7%. The rest of 6.3% can be attributed to the effects of other factors, namely: volumetric fraction of biocatalyst particles, sparger position, ratio of cross areas of riser and downcomer flow regions, height of gas separation or bottom clearance regions, etc.

The studies on mixing intensity and distribution for immobilized *Y. lipolytica* suspensions in a split-cylinder gas-lift bioreactor underlined that the mixing efficiency increased along the riser region height, from the bioreactor bottom to its top. The lowest values of mixing time have been recorded for the alginate particles with the intermediary diameter of 3.6 mm. However, for the top position, at air superficial velocity

higher than $1.05x10^{-3}$ m/s, the most efficient mixing corresponded to the largest biocatalyst particles, of 4.2 mm diameter.

The distribution of mixing intensity in the downcomer zone is different, the highest turbulence being induced in the intermediary positions for immobilized yeast particles with 4.2 mm diameter. The positive influence of aeration rate on turbulence extent was recorded only for air superficial velocity up to $1.35x10^{-3}$ m/s. For higher values of air input rate, the phenomenon of bubbles entrapping in the downward flow became significant, this leading to the hindrance of broth circulation and, implicitly, to the increase of mixing time especially for the smallest or intermediary size biocatalysts.

The influences of the considered factors on mixing intensity have been included in two mathematical correlations established separately for the riser and downcomer regions. The proposed equations allow predicting the mixing time on the height of the internal-loop gas-lift for these two circulation regions of bioreactor and offer a good agreement with the experimental results.

A. NOTATIONS

B. d_P - biocatalyst particle diameter, m
C. h - distance from the bioreactor bottom, m
D. t_m - mixing time, s
E. v_S - air superficial velocity, m/s
F. α, β, γ, δ - parameters of equation (2)

G. 4. SELECTED REFERENCES

1. Caşcaval D., Galaction A.-I., Marius Turnea, Lupăşteanu A.-M., (2012), Biodegradation of lipids from olive oil mill wastewaters in a stationary basket bioreactor with immobilized *Bacillus spp.* cells – Influence of internal diffusion, *Water Science and Technology*, 65(5), 920-926.

2. Caşcaval, D., Galaction, A. I., Turnea, M. (2007). Comparative analysis of mixing distribution in aerobic stirred bioreactor for simulated yeasts and fungus broths, *J. Ind. Microbiol. Biotechnol.*, 34, 35-47.

3. Caşcaval, D., Matran, R. M., Turnea, M., Blaga, A. C., Galaction, A. I. (2015). Distribution of mixing efficiency in a split-cylinder gas-lift bioreactor for Yarrowia lipolytica *suspensions*, *Can. J. Chem. Eng.*, 93, 18-28.

4. Chakraborty, D., Guha, M., Banerjee, P. K. (2009). CFD simulation on influence of superficial gas velocity, column size, sparger arrangement, and taper angle on hydrodynamics of the column flotation cell, *Chem. Eng. Commun*., 196, 1102-1116.

5. Chipasa K.B., Medrzycka K., (2006), Behavior of lipids in biological wastewater treatment process, *Journal of Industrial Microbiology & Biotechnology*, 33, 635-645.

6. Daims H., Taylor M.W., Wagner M., (2006), Wastewater treatment: a model system for microbial ecology, *Trends in Biotechn*ology, 24, 483-489.

7. Deive, F. J., Sanroman, M. A., Longo, M. A. (2010). A comprehensive study of lipase production byYarrowia lipolytica CECT 1240 (ATCC 18942): from shake flask to continuous bioreactor, *J. Chem. Technol. Biotechnol*., 85, 258-266.

8. Galaction A.-I., Matran R.-M., Blaga A.-C., Turnea M., Caşcaval D., (2014), Applications of pneumatic bioreactors in wastewaters treatment 1. Mixing efficiency and distribution in split-cylinder gas-lift bioreactor for viscous media, *Environmental Engineering Management Journal*, 13, 2653-2664.

9. Galaction, A. I., Lupăşteanu, A. M., Caşcaval, D. (2007). Bioreactors with stirred bed of immobilized cells. 1.Studies on mixing efficiency, *Environ. Eng. Manag. J.*, 6, 101-110.

10. Gavrilescu M., Chisti Y., (2005), Biotechnology - a sustainable alternative for chemical industry, *Biotechnology Advances*, 23, 471-499.

11. Lan W., Gang G.E., Jinbao W., (2009), Biodegradation of oil wastewater by free and immobilized *Yarrowia lipolytica* W29, *Journal of Environmental Sciences*, 21, 237-242.

12. Martinez-Garcia, G., Johnson, A. C., Bachmann, R.T., Williams C. J., Burgoyne A., Edyvean R. G. J. (2009). Anaerobic treatment of olive mill wastewater and piggery effluents fermented with *Candida tropicalis*, *J. Hazard. Mater.*, 164, 1398-1405.

13. Nienow, A. W. (1997), On impeller circulation and mixing effectiveness in the turbulent flow regime, *Chem. Eng. Sci.*, 52, 2557-2565.

14. Pavlostathis S.G., Giraldo-Gomez E., (1991), Kinetics of anaerobic treatment, *Water Science and Technogy*, 24, 35-59.

15. Van't Riet K., Tramper, J. (1991). *Basic Bioreactor Design*, M. Dekker Inc., New York

16. Williams, D., Munnecke, D. M. (1981). The production of ethanol by immobilized yeast cells. *Biotechnol. Bioeng*, 23, 1813-1825.

17. Zeeman G., Sanders W., (2001), Potential of anaerobic digestion of complex wastewater, *Water Science and Technology*, 44, 115-122.

2. SYNTHESIS OF ENANTIOPURE L-(5-PHENYLFURAN-2-YL)ALANINES BY A SEQUENTIAL MULTIENZYME PROCESS

Unnatural amino acids, the non-genetically-coded amino acids that either occur naturally or are chemically synthesized, are becoming very important tools for modern drug discovery research. Due to their structural diversity and functional versatility, they are widely used as chiral building blocks and molecular scaffolds in constructing combinatorial libraries, especially in the synthesis of peptides with enhanced properties (e.g. proteolytic stability, biological activity, etc).[1] They are also commonly used as moiety in the rational design of chiral drugs such as anti-cancer compounds[2] and viral inhibitors[3] or as key intermediates of pharmaceuticals from broad range of therapeutic fields such as hypertension, diabetes, HIV, migraine, etc.[4] Several non-proteinogenic amino acids as L-Dopa, L-homophenylalanine or D-2-naphtylalanine are on their own important pharmaceuticals[5] while others as D-phenylglycine, D-*para*-hydroxyphenylglycine, 2-thienylalanine, etc. are useful for the synthesis of certain drugs.[6] Accordingly, the enantioselective synthesis of amino acids is an attractive goal. While natural L-amino acids are obtained by fermentation or applying natural enzymatic systems, for the synthesis of enantiopure unnatural amino acids, chiral chemical catalysis or biocatalysis is employed. Among the most common enantioselective synthetic procedures – such as reductive amination, transamination, asymmetric hydrogenation, kinetic resolution[7] – the biocatalytic approaches based on the use of aminoacylases, hydantoinases, aminotransferases, ammonia- lyases and amino acid dehyrogenases offer valuable synthetic alternatives.[8] Despite the success of enzyme catalyzed kinetic resolutions for the synthesis of a wide range of chiral building blocks, there is an increasing demand to develop transformations which are not limited by a maximum yield of only 50% of the desired enantiomer of the product. Increasing attention has been given in recent years to the development of dynamic kinetic resolution (DKR) processes[9] in which the unreactive enantiomer equilibrates *in situ* under the reaction conditions, with the more reactive antipode. DKR reactions can thus result in quantitative yields, with enantiomeric excesses approaching 100%.

The first enzymatic DKR of oxazol-5-(4*H*)-one was reported in 1990.[10] It was shown that, due to the *in situ* racemization of the substrate during the Lypozyme TLIM-catalyzed butanolysis of 2-phenyl-4-methyl-oxazol-5-(4*H*)-one, the *N*- and *C*- protected (*S*)-alanine was formed with moderate enantiomeric excess but with 100% conversion. It was demonstrated in this way that oxazolones were excellent substrates for stereoselective DKR due to the low p*Ka* of the C-4 proton and their inhered reactivity towards lipase-catalyzed alcoholysis.[11] Furthermore, the same procedure was found to be adequate for the enzymatic DKR of other 4-substituted 2-phenyloxazol-5(4*H*)-ones and it was also shown that the nature of the solvent influenced the stereoselectivity of the reaction.[12] The efficiency of enzymatic DKR of oxazolones was further improved by using catalytic amounts of organic bases in the reaction media enhancing the racemization rate of the substrates and the enantiomeric excesses of the isolated products.[13,14]

A reliable chemo-enzymatic procedure for the preparation of enantiopure benzofuranyl- and benzothiophenyl-alanines, starting from racemic 2-acetamido-3-(heteroaryl)propanoic acids was previously described by us[14], involving the Novozyme 435-mediated dynamic kinetic resolution of the oxazolones which provided with 100% conversion the *N*- and *C*-protected L-amino acids. It was shown that the spontaneous racemization of these oxazolones was faster than the enzymatic alcoholysis, avoiding the need of an organic base in the reaction media. This unexpected feature of the mentioned 4-heteroaryl-2-methyl-oxazol-5(4*H*)-ones in relation to all other previously reported examples, prompted us to investigate the behavior of 5-phenyl-furan-2-yl based heteroaryloxazolones in their lipase catalyzed DKR in order to set up an optimized chemoenzymatic procedure for the preparative-scale synthesis of the corresponding optically pure L-(5-phenyl-furan-2-yl)-alanines.[14] This methodology would be more accessible for synthetic chemists, compared to the previously described[15] phenylalanine ammonia lyase (PAL) mediated stereoselective ammonia addition to (5-phenyl-furan-2-yl)-acrylates.

A. Results and discussion

Chemical synthesis

5-Aryl-furan-2-carbaldehydes were used as starting materials. Their transformation via rac-2-acetamido-3-(5-phenylfuran-2-yl)propanoic acids (rac-**1a-d**) into racemic amino acids rac-**4a-d** was performed in accordance with the malonic synthesis protocol. Both racemic oxazolones rac-**3a-d** and racemic 2-acetamido-3-(5-phenyl-furan-2-yl)propanoic acid esters (rac-**2a-d**) were obtained from rac-**1a-d** using the methodology previously reported by us.[14] (Scheme 2.1).

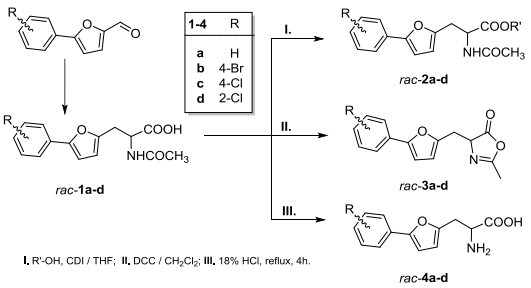

Scheme 2.1. Synthesis of racemic heteroarylalanines and their derivatives

Enzymatic synthesis

To investigate the stereoselectivity and the optimal conditions of DKR for the lipase mediated alcoholysis of 4-[(5-phenyl-furan-2-yl)methyl]-2-methyloxazol-5(4*H*)-ones *rac*-**3a-d** followed by the transformation of the 2-acetamido-3-(5-phenylfuran-2-yl)propanoic acid esters (*rac*-**2a-d**) into enantiopure amino acids L-**4a-d**, the chromatographic separation of the enantiomers of *rac*-**1-4-a-d** was first established as shown in detail in the experimental section.

A large number of commercial available lipases exhibit high substrate tolerance, leading to products with various degrees of enantioselectivity. Accordingly, in order to obtain L-2-acetamido-3-(5-phenylfuran-2-yl)propanoic acid esters L-**2a-d** in good yields and high selectivities, several enzymes were tested as potential biocatalysts for the DKR of *rac*-**3a-d** (Scheme 2.2a). The reactions were first performed in neat anhydrous alcohols at room temperature. Four different alcohols (methanol, ethanol, propan-1-ol and butan-1-ol) were used as solvent and nucleophile. All lipases showed the same enantiopreference for the alcoholysis, although their behavior greatly differed. While CaL-A and CrL were catalytically inactive, Lipozyme from *Mucor miehei* (LMM), PPL and lipase AK showed moderate selectivity (enantiomeric excesses of 20-49%) and reactivity (5-10% conversion, after 24 hours) in all tested alcohols. Only CaL-B adsorbed on macroporous acrylic resin (Novozyme 435) showed acceptable properties, displaying higher selectivities in ethanol as shown in Table 2.1.

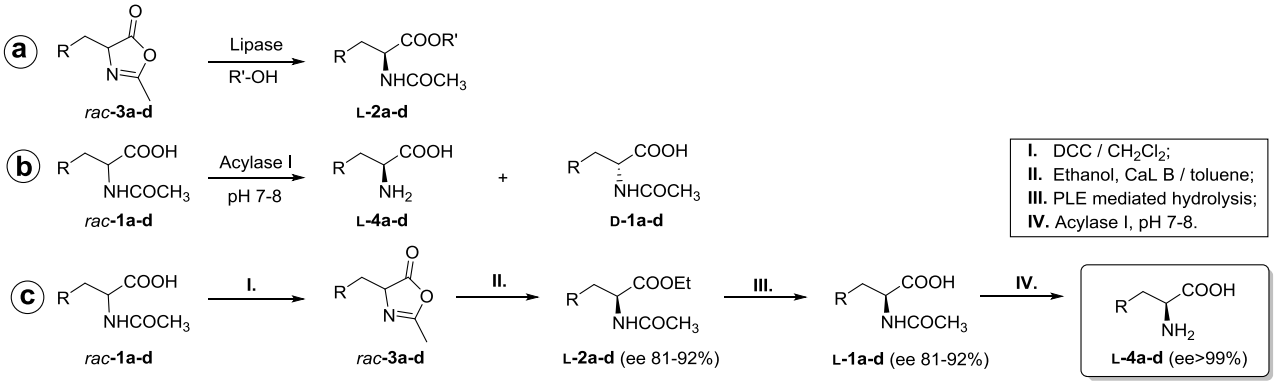

Scheme 2.2. Enantioselective synthesis of L-heteroarylalanines and their derivatives: (a) DKR of the lipase mediated alcoholysis of oxazolones *rac*-**3a-d**; (b) enantiomer selective hydrolysis of *rac*-**1a-d**; (c) chemoenzymatic synthesis of enantiopure L-**4a-d**.

The decreasing enantiopurities of the produced L-**2a-d** with increasing reaction conversions indicated that the optimal conditions for an efficient DKR were not been satisfied. From the elution diagrams of samples taken periodically from the reaction mixture it was found that the complete transformation of *rac*-**3a-d** into L-**2a-d** was not accompanied by the efficient spontaneous racemization of oxazolones. With other words, the enzymatic reactions of the less reactive enantiomer were faster than racemization of substrates.

For an efficient enzymatic dynamic kinetic resolution three general requirements must be meet simultaneously, namely: the enzyme must stay active throughout the reaction, the less reactive enantiomer must undergo rapid racemization under the reaction conditions where the product of the enzyme-catalyzed reaction is stable and finally, the racemizing agent should not catalyze non-enzymatic secondary reactions, which could decrease the enantiopurity of the desired product. In this way, the substrate should be always racemic, allowing the maximal enantiopurity at the theoretical zero conversion of the more reactive enantiomer; in this way the ee of the product will be constant during the reaction. This is mandatory for an enzymatic reaction with low or medium stereoselectivity since the ee of the product will decrease with

increasing conversion in KR or an inefficient DKR. Moreover, the nature of the solvent could significantly influence the activity and selectivity of the enzymatic reaction

Table 2.1. Novozyme 435-catalyzed ring opening of *rac*-**3a-d** in neat alcohols

Entry	Substrate	Solvent/ Nucleophile	Product	*ee* After 2h	c^a	*ee* After 12 h	c^a
1	*rac*-**3a**	methanol	L-**2a**	70	6	64	21
2		ethanol		91	8	72	62
3		propan-1-ol		87	7	79	58
4		butan1-ol		87	5	81	49
5	*rac*-**3b**	methanol	L-**2b**	55	5	33	20
6		ethanol		88	8	52	66
7		propan-1-ol		80	7	55	57
8		butan1-ol		78	5	48	44
9	*rac*-**3c**	methanol	L-**2c**	58	5	37	18
10		ethanol		91	8	81	44
11		propan-1-ol		78	8	70	41
12		butan1-ol		77	9	72	40
13	*rac*-**3d**	methanol	L-**2d**	25	3	18	23
14		ethanol		79	5	67	33
15		propan-1-ol		62	5	58	19
16		butan1-ol		70	6	65	17

[a] approximate conversions calculated from the uncorrected chromatographic peaks area (HPLC) of the reaction counterparts

. Accordingly, CaL-B as catalyst and ethanol as nucleophile were used in several solvents for further studies. It was previously shown[12-14] that the enzymatic dynamic kinetic resolution of 4-substituted *rac*-2-phenyloxazol-5(*4H*)-ones could be influenced (altered enzyme activity and selectivity) by the presence of water and by the nucleophile-substrate and enzyme-substrate *ratio*. The presence of water can generate a carboxylic acid which in turn can interact with the enzyme, changing its conformation, which can result in a decrease of the ee. In order to overcome this problem all the reactions were carried out under anhydrous conditions and before use the enzymes were dried or crashed and dried, as described by Turner *et al.*[13.] For high selectivity and good reactivity, first the potential effect of the CaL-B's residual water content upon the hydrolysis of *rac*-**3a-d** was investigated in various solvents in the absence of the selected nucleophile (ethanol). Even after 3 days no trace of any product was found in the reaction mixtures. Further, keeping the same substrate: catalyst *ratio* in presence of 2, 4, 6, 8 and 10 equiv. of ethanol, the CaL-B mediated DKR of *rac*-**3a-d** was performed in several organic solvents (data not shown). It is important to note that in the enzyme-less control experiments, even after 48 h shaking, no trace of any products of chemical reaction (hydrolysis or ethanolysis) were chromatographically detected. By far toluene proved to be the most appropriate solvent for all substrates in terms of stereoselectivity, but also the enzyme activity was higher than in experiments performed in neat ethanol. Highest enzymatic DKR velocity was detected when 6 equiv. of ethanol was used as nucleophile. As it was expected, also for DKR's performed in toluene the spontaneous but incomplete racemization of oxazolones *rac*-**3a-d** during the reaction was observed. Consequently, the detected high values of enantiomeric excesses of L-**2a-d** at low conversions decreased constantly with the increase of the conversion, yielding L-**2a-d** with unsatisfactory enantiopurities, as shown in Table 2.2.

For the efficient production of highly enantiomerically enriched ethyl L -(2-acetamino-3-(5-phenylfuran-2-yl))propano-ates L-**2a-d** (Scheme 2.2), the presence of a proper base at an appropriate concentration in the reaction mixture is essential.

Table 2.2. CaL-B catalyzed complete conversion of *rac*-**3a-d** with ethanol (6 equiv.) in toluene as solvent

Entry	Substrate	Product	*ee* (%)[a]	Time (h)[a]
1	*rac*-**3a**	L-**2a**	78	8
2	*rac*-**3b**	L-**2b**	63	12
3	*rac*-**3c**	L-**2c**	70	12
4	*rac*-**3d**	L-**2d**	57	16

[a] complete consumption of the substrate

The selected base should keep the starting material in racemic form during the enzymatic reaction but it should not catalyze the chemical ethanolysis of the substrate and it should not decrease mostly the selectivity but also the activity of the enzyme. The catalytic activity of various aliphatic (diethyl-amine,

triethyl-amine, triethanol-amine, diethyl-ethanolamine), aromatic (diethyl-aniline,benzyl(-diethyl)-amine) and heteroaromatic amines (pyridine and 4-(dimethyl-4-amino)-pyridine) were tested (each in 0.5 equiv.) in enzyme-less control reactions. Except pyridine and 4-(dimethyl-4-amino)-pyridine, which proved to be catalysts for the chemical ethanolysis of *rac*-**3a-d**, all the other bases showed no catalytic activity for the same undesired non-enzymatic reactions, consequently they were further tested as potential racemizing agents in the enzymatic DKRs. While diethyl-amine proved to be a strong inhibitor of the enzyme, the aromatic amines were inefficient in the racemization procedure. Since all the other tested aliphatic amines were proper for our scope, triethyl-amine (a highly volatile amine involving facile work-up procedures for the preparative-scale reactions) was selected as racemizing agent.

Table 2.3. CaL B-catalyzed preparative scale DKR of *rac*-**3a-d** with ethanol (2 equiv.) in toluene using triethylamine (0.25 equiv.) as racemizing agent

Entry	Substrate	Product	*ee* [a] (%)	Time (h)
1	*rac*-**3a**	L-**2a**	92	2
2	*rac*-**3b**	L-**2b**	84	3
3	*rac*-**3c**	L-**2c**	85	3
4	*rac*-**3d**	L-**2d**	81	5

[a] complete consumption of the substrate

Comparing the ee of the formed ethyl L-[2-acetamino-3-(5-phenyl-furan-2-yl)]propanoates L-**2a-d** at small conversion in the base-less enzymatic ethanolysis and in the DKR in presence of triethyl-amine, it was found that the racemizing agent slowly decreased the selectivity of the enzyme.

Further, by the concomitant decreasing of the previously fixed nucleophile (6 equiv.) and base (0.5 equiv.) concentrations, the use of 2 equiv. of ethanol in presence of 0.25 equiv. of triethyl-amine in toluene was found as optimal condition for the CaL-B catalyzed DKR of *rac*-**3a-d** (Table 2.3).

For the deprotection of the enantiomerically enriched L-2-acetamido-3-(5-phenyl-furan-2-yl)propanoic acids ethyl esters L-**2a-d**, two regioselective hydrolytic steps were required: the ester hydrolysis followed by amide hydrolysis. Even the mild chemical hydrolysis of the ester moiety of L-**2a-d** with sodium bicarbonate at room temperature underwent with partial racemization, decreasing the ee of the formed L-**1a-d** compared with the ee of the starting L-**2a-d**. To overcome this drawback the PLE catalyzed hydrolysis of the ester moiety was applied in dioxane-water (1:1, vv/v) mixture. Moreover, Acylase I-mediated kinetic resolution of racemic 2-acetamido-3-aryl-propanoic acids *rac*-**1a-d** yielded enantiopure L-2-amino-3-(5-phenylfuran-2-yl)propanoic acids L-**4a-d** and D-2-acetamido-3-(5-phenyl-furan-2-yl)propanoic acids D-**1a-d** at small scale as well as at preparative scale (Scheme 2.2b).

Further, the preparative scale synthesis of the enantiopure L-**4a-d** from racemic 2-acetamido-3-(5-phenyl-furan-2-yl)propanoic acids *rac*-**1a-d** was set up (Scheme 2.2c). The progress of the reaction was monitored after each step by HPLC, in order to determine the enantiopurities of the isolated compounds and the conditions for quantitative conversions. The lipase-mediated DKR was stopped when the consumption of the *rac*-2-methyl-4-[(5-phenyl-furan-2-yl)methyl]oxazol-5(4*H*)-ones *rac*-**3a-d** was complete. The ee of the isolated products was slightly decreased compared with those found for the small scale reactions. Then, by PLE-mediated hydrolysis, the L-2-acetamido-3-(5-phenyl-furan-2-yl)propanoic acid propyl esters L-**2a-d** were transformed with good yields (~98%), without altering the ee, into L-2-acetamido-3-(5-phenylfuran-2-yl)propanoic acids L-**1a-d**. Next, through the highly enantiomer selective Acylase I-mediated hydrolysis of the latest compounds, the enantiopure L-alanines L-**4a-d** were isolated. The yields and the specific optical rotation values of the isolated final products are shown in Table 2.4.

Table 2.4. Yields and optically rotatory power for the isolated enantiopure L-alanines L-**4a-d**.

Substrate	Product	Yield [a] (%)	$[\alpha]_D^{25}$ [b]
rac-**1a**	L-**4a**	84	+28.2
rac-**1b**	L-**4b**	81	+10.8
rac-**1c**	L-**4c**	80	+17.8
rac-**1d**	L-**4d**	82	+16.7

[a] Global yield, based on the starting *rac*-**1a-d**; [b] 10 mg mL^{-1}; ee > 99% for all compounds; in CH_3COOH at 25 °C

B. Experimental part

Analytical methods

The ^{1}H- and ^{13}C-NMR spectra were recorded on a Bruker Advance spectrometer operating at 300 and 75 MHz, at 25 °C. Electron impact mass spectra (EI-MS) were taken on a LCQ advantage by ThermoFisher spectrometer operating at 1950-2050V, using samples dissolved in MeOH:H_2O 1:1 (v/v) or MeOH:CH_3CN 1:1 (v/v).

High Performance Liquid Chromatography (HPLC) analyses were conducted with an Agilent 1200 instrument using an Astec Chirobiotic-Tag column (4.6×250 mm) and a mixture of methanol and TEAA buffer (pH 4.1), 80:20 (v/v) as eluent for enantiomeric separation of *rac*-**1,4a-d**, a Chiralpak IA column (4.6×250 mm) and a mixture of hexane and propan-2-ol, 90:10 (v/v) as eluent for enantiomeric separation of *rac*-**2,3-a,c,d**, a Chiralpak IC column (4.6×250mm) and a mixture of hexane: propan-2-ol, 90:10 (v/v) as eluent for enantiomeric separation of *rac*-**2,3b**, at 1 mL min^{-1} flow rate in all cases. For all chiral compounds, high resolution enantiomeric separations were performed. Retention times for L- and D-**1-4a-d** are presented in Table 2.5.

Thin Layer Chromatography (TLC) was carried out using Merck Kieselgel 60F_{254} sheets. Spots were visualized by treatment with 5% ethanolic phosphomolybdic acid solution and heating. Preparative chromatographic separations were performed using column chromatography on Merck Kieselgel 60 (63-200 μm). Melting points were determined by hot plate method and are uncorrected. Optical rotations were determined on a Perkin-Elmer 201 polarimeter and $[\alpha]_D^{20}$ values are given in units of 10^{-1} deg cm^2 g^{-1}.

Table 2.5. Retention times of the enantiomers of *rac*-**1-4a-d**.

				R_t **(min.)**			
L-**1a**	D-**1a**	L-**1b**	D-**1b**	L-**1c**	D-**1c**	L-**1d**	D-**1d**
10.90	3.20	13.61	3.32	12.69	3.22	12.89	3.68
L-**2a**	D-**2a**	L-**2b**	D-**2b**	L-**2c**	D-**2c**	L-**2d**	D-**2d**
13.04	9.63	38.99	34.95	15.81	10.06	10.84	8.48
3a		**3b**		**3c**		**3d**	
8.33	11.12	9.25	10.41	9.93	12.99	7.80	10.48
L-**4a**	D-**4a**	L-**4b**	D-**4b**	L-**4c**	D-**4c**	L-**4d**	D -**4d**
9.04	13.92	9.72	16.16	9.17	15.40	10.23	15.40

Reagents, solvents and biocatalysts

All inorganic reagents and solvents were products of Aldrich or Fluka. All solvents were purified and dried by standard methods as required. Lipase AK was from Amano, Europe. Lipases from *Candida rugosa* (CrL), Lypozyme from *Mucor miehei* (LMM), Lipase from porcine pancreas (PPL) and Acylase I were purchased from Fluka and pig liver esterase (PLE) from Sigma-Aldrich. Lipase B (CaL-B, Novozyme 435) and Lipase A (CaL-A) from *Candida antarctica* were purchased from Novozymes, Denemark.

CHEMICAL SYNTHESIS OF RACEMIC ALANINES AND THEIR DERIVATIVES

*Synthesis of rac-2-acetamido-3-(5-phenyl-furan-2-yl)pro-panoic acids rac-**1a-d***

The racemic 2-acetamido-3-aryl-propanoic acids *rac*-**1a-d** were synthetized from the corresponding 5-phenylfuran-2-carbaldehydes prepared by Meerwein method[16] using a known procedure.[15]

*Synthesis of racemic ethyl 2-acetamido-3-(5-phenyl-furan-2-yl)propanoates rac-**2a-d***

Into a solution of *N,N'*-carbonyldiimidazole (90 mg, 0.55 mmol) and *rac*-2-acetamido-3-(5-phenyl-furan-2-yl)propanoic acid *rac*-**1a-d** (0.5 mmol) in anhydrous THF (2.5 mL), ethanol (45 mg, 56 μL, 0.75 mmol) was added in one portion at room temperature. After the reaction was completed (checked by TLC), the solvent was distilled off *in vacuo* and the crude product was purified by column chromatography on silica gel using as eluent dichloromethane-acetone 90:10 (v/v). Methyl, ethyl and butyl 2-acetamido-3-(5-phenyl-furan-2-yl)propanoates were prepared in the same manner.

*Synthesis of rac-2-meyhyl-4-[(5-phenyl-furan-2-yl)-2-methyl]oxazol-5(4H)-ones rac-**3a-d***

Into a solution *rac*-2-acetamido-3-aryl-propanoic acid (*rac*-**1a-d**) (0.5 mmol) in anhydrous dichloromethane (5 mL), a solution of dicyclohexylcarbodiimide (135 mg, 0.6 mmol) in anhydrous dichloromethane (2 mL) was added dropwise at 0°C. Before the addition was completed, 1,3-dicyclohexylureea started to precipitate. Reaction mixture was further stirred for 5-10 min. At the end the solid was filtered off and dichloromethane was removed under reduced pressure at room temperature yielding the desired product. The obtained *rac*-4-((5-phenyl-furan-2-yl)methyl)-2-methyl-oxazol-5(4*H*)-one (*rac*-**3a-d**) was immediately used in enzymatic reactions without further purification.

*Synthesis of rac-2-amino-3-(5-phenyl-furan-2-yl)-propanoic acids rac-**4a-d***

The *rac*-2-acetamido-3-aryl-propanoic acid *rac*-**1a-d** (1 g) was suspended in half concentrated HCl (10 mL) and the mixture was refluxed for 4 h, followed by the removal of the solvent *in vacuo*. The crude product was washed with diethyl ether (3×10 mL), filtered and dried, giving the pure product.

ENZYME REACTIONS AT SMALL SCALE

Dynamic kinetic resolution of rac-2-meyhyl-4-[(5-phenyl-furan-2-yl)-2-methyl]oxazol-5(4H)-ones (rac-3a-d) by enzymatic alcoholysis

In a typical small scale experiment, one of the tested lipases (10 mg) was added to the solution of *rac-2-meyhyl-4-[(5-phenyl-furan-2-yl)-2-methyl]oxazol-5(4H)-one* (*rac*-**3a-d**) (10 mg) in different alcohols (methanol, ethanol, propan-1-ol, butan-1-ol; 1 mL) and the mixture was stirred at room temperature. Samples (10 μL) were taken periodically, diluted with hexane: propan-1-ol (9:1, 990 μL) and analyzed by HPLC as described in section 4.1.

For improving the ee, different solvents were used as reaction media: CaL B (10 mg) was added into a solution of *rac-2-meyhyl-4-[(5-phenyl-furan-2-yl)-2-methyl]oxazol-5(4H)-one* (*rac*-**3a-d**) (10 mg) in different kinds of solvents (1 mL) and different equiv. (2 ,4, 6, 8, 10) of ethanol was added. The mixture was stirred at room temperature and samples (10 μL) were taken, diluted with hexane: propan-2-ol (9:1, 990 μL) and analyzed by HPLC in the same manner.

Kinetic resolution of racemic 2-acetamido-3-(5-phenyl-furan-2-yl)propanoic acids (rac-1a-d) by hydrolysis with Acylase I

rac-2-Acetamido-3-(5-phenylfuran-2-yl)propanoic acid (*rac*-**1a-d**) (0.5mmol) was suspended in water (5 mL). By adjusting the pH to 7.5-8 with LiOH solution (1.25 M), the suspension was dissolved. Then Acylase I (2.5 units, 6 mg) and $CoCl_2 \times 6H_2O$ (2.5 mg, 0.02 mmol) was added and the reaction mixture was stirred at 37 °C, while by additions of LiOH solution (1.25 M), the pH of the solution was permanently kept between 7 and 8. After the completion of L-2-acetamido-3-arylpropanoic acid (L-**1a-d**) hydrolysis (approx. 24 h, checked by HPLC) the pH was adjusted to 1.5 with 5% HCl solution. The unreacted enantiopure D-2-acetamido-3-aryl-propanoic acid (D-**1a-d**) was filtered off and washed with deionized water (3×1 mL). The filtrate was heated with active charcoal (10 mg) to 60 °C for 1 min, cooled to room temperature, filtered, and applied to a Dowex 50X8 cation exchange resin column. Elution of the pure L-enantiomer of the 2-amino-3-aryl-propanoic acid (L-**4a-d**) occurred with 2M ammonia solution.

Large scale enzymatic preparation of enantiopure L-2-amino-3-(5-phenyl-furan-2-yl)propanoic acids (L-4a-d)

Into a solution *rac*-2-acetamido-3-(5-phenyl-furan-2-yl)propanoic acid (*rac*-**1a-d**) (5 mmol) in anhydrous dichloromethane (50 mL), a solution of dicyclohexyl-carbodiimide (1350 mg, 6 mmol) in anhydrous dichloromethane (50 mL) was added dropwise at 0°C. The reaction mixture was stirred for 5-10 min, the formed solid was filtered off and dichloromethane was removed under reduced pressure at room temperature.

The formed *rac-2-meyhyl-4-[(5-phenyl-furan-2-yl)-2-methyl]oxazol-5(4H)-one* (*rac*-**3a-d**) was dissolved in toluene (65 ml) followed by the addition of CaL-B (1300 mg) and ethanol (600 mg, 750 μL, 10 mmol). The mixture was stirred at room temperature, until the ethanolysis of *rac-2-meyhyl-4-[(5-phenyl-furan-2-yl)-2-methyl]oxazol-5(4H)-one* (*rac*-**3a-d**) completed (reaction followed by HPLC as described). The enzyme was filtered off and the solvent was removed under reduced pressure to yield L-**2a-d** as semisolid. L-**2a-d** was dissolved in dioxane-water (10 mL, 1:1, v/v) and after addition of PLE (500 mg) the mixture was stirred for 12 h at room temperature. The mixture was concentrated *in vacuo* and the crude product was extracted with dichloromethane and water (3×10 mL each solvent), successively. The aqueous phase was then acidified carefully with conc. HCl solution. The deposited precipitate was filtered off and washed several times with cold water. The isolated L-2-acetamido-3-(5-phenyl-furan-2-yl)propanoic acid (L-**1a-d**) was dissolved in water (10 mL) by adjusting the pH to 7.5-8 with LiOH solution (1.25 M). Then Acylase I (22 units, 60 mg) and $CoCl_2 \times 6H_2O$ (50 mg, 0.2 mmol) were added and the reaction mixture was stirred at 37 °C,

while the pH of the solution was kept between 7 and 8, by addition of LiOH solution (1.25 M). After the hydrolysis of L-2-acetamido-3-(5-phenylfuran-2-yl)propanoic acid (L-**1a-d**) completed, the pH was adjusted to 1.5 with 5 % HCl. The formed suspension was extracted with dichloromethane (3×10 mL). The aqueous phase was heated with active charcoal (50 mg) to 60 °C for 1 min., cooled at room temperature, filtered and applied to a Dowex 50X8 cation exchange resin column. Elution of the pure L-enantiomers of the 2-amino-3-(heteroaryl)-propanoic acids (L-**4a-d**) occurred with 2M ammonia solution.

In conclusion, An efficient multi-enzyme process for the preparation of enantiopure arylalanines L-4a-d, starting from racemic 2-acetamido-3-(5-phenyl-furan-2-yl)propanoic acids *rac*-1a-d, in high yields is described. First, the dynamic kinetic resolution of the racemic oxazolones mediated by CaL-B provided quantitatively the *N*- and *C*-protected L-amino acids L-2a-d (68-92% ee). The protective groups were removed in excellent yields by a second (mild PLE-mediated hydrolysis of the ester group) and a third enzymatic step (Acylase I catalyzed stereoselective hydrolysis of the amide group). The latest step, due to the L-specificity of Acylase I, raised the ee of the final products to more than 99 %.

References

1. (a) Whitby, L.R; Boger, D.L. *Acc. Chem. Res.* **2012**, 45, 1698-1709; (b) Stevenazzi, A.; Marchini, M.; Sandrone, G.; Vergani, B.; Lattanzio, M. *Bioorg. Med. Chem. Lett.* **2014**, *24*, 5349-5356.
2. (a) Kumar, Vivek; Mudgal, Mukesh M.; Rani, Nidhi; Jha, Amrita; Jaggi, Manu; Singh, Anu T.; Sanna, Vinod K.; Singh, Pratibha; Sharma, Pramod K.; Irchhaiya, Raghuveer; Burman, Anand C. *J. Enzyme Inhib. Med. Chem.* **2009**, *24(3)*, 763-770; (b) Xin Deng, Qianqian Qiu, Baowei Yang, Xuekun Wang, Wenlong Huang, Hai Qian, *Eur. J. of Med. Chem.* **2015**, *89*, 540-548; (c) Hasabelnaby, S.; Goudah, A.; Agarwal, H.K.; Abdalla, M.A.; Tjarks, W. *Eur. J. of Med. Chem.* **2012**, *55*, 325-334.
3. (a) Yuzeng; L.; Ashoke, S.; Grier, J.P.; Rapp, K.L.; Schinazi, R.F.; Chu, C. K. *Bioorg. Med. Chem.* **2009**, *17(3)*, 1404-1409; (b) Kati, W.M.; Montgomery, D.; Maring, C.; Stoll, V.S.; Giranda, V.; Chen, X.; Laver, W.G.; Kohlbrenner, W.; Norbeck, D.W. *Antimicrob. Agents Chemother* **2001**, *45(9)*, 2563-70.
4. (a) Barbosa, O.; Ortiz, C.; Torres, R.; Fernandez-Lafuente, R. *J. Mol. Catal. B: Enzymatic* **2011**, *71*, 124–132; (b) Krapcho, J.; Turk, C.; Cushman, D.W.; Powell., J.R.; DeForrest, J.M.; Spitzmiller, E.R.; Karanewsky, D.S.; Duggan, M.; Rovnyak, G. *J. Med. Chem.***1989**, 31, 1148–1160; (c) Stinson, S. C. *Chem. Eng. News* **1995**, *73*, 44–74; (d) Bajusz, S.; Széll, E.; Bagdy, D.; Barabás, E.; Horváth, G.; Diószegi, M.; Fittler, Z.; Szabó, G.; Juhász, A. *J. Med. Chem.* **1990**, *33*, 1729–1735; (e) Kempf, D.J.; Codacovi, L.M.; Norbeck, D.W.; Plattner, J.J.; Sham, H.L.; Wittenberger, S. *US Patent Application* 486948, **1991**; (f) Patel, R.N. *Biomol. Eng.* **2001**, *17*, 167-182.
5. (a) Servi, S.; Tessaro, D.; Pedrocchi-Fantoni G. *Coord. Chem. Rev.* **2008**, *252*, 715-726; (b) Lipski, J.; Nistico, R.; Berretta, N.; Guatteo, E.; Bernardi, G.; Mercuri, N.B. *Progr. Neurobiol.* **2011**, *94*, 389-407.
6. (a) Zaks, A.; Dodds, D. R. *Drug Discovery Today* **1997**, 513-532; (b) Lilley, M.; Mambwe, B.; Jackson, F.W.; Muimo, R. *Chem. Commun.* **2014**, 50, 9343-9345.
7. (a) Byung-Kwan, C.; Joo-Hyun, S.; Tae-Won, K.; Byung-Gee, K. *Biotechnol. Bioeng.* **2003**, *83*, 226 –234; (b) da Silva, M.R,; de Mattos, M.C.; da Conceição Ferreira de Oliveira, M.; Gomes de Lemos, T.L.; Pontes, N.M.; Silva R., de Gonzalo, G.; Lavandera, I.; Gotor-Fernández, V.; Gotor, V. *Tetrahedron* **2014**, *70*, 2264-2271.
8. (a) Rui-Lin, G.; Ik-Soo, L., Charles. J.S. *Tetrahedron Letters* **1992**, *33*, 1953-1956; Wegman, M.A.; Janssen, M.H.A.; van Rantwijk, F.; Sheldon, R.A. *Adv. Synth. Catal.* **2001**, *343*, 559–576; (b) Koksch, B.; Quaedflieg, P.J.L.M.; Michel, T.; Burger, K.; Broxterman, Q.B.; Schoemaker, H.E. *Tetrahedron: Asymmetry* **2004**, *15*, 1401–1407; (c) Bommarius, A.S.; Drauz, K.; Groeger, U.; Wandrey, C. In *Chirality in Industry*; John Wiley &Sons Ltd., **1992**, pp 371–397; (d) Poppe, L., Rétey, J., *Angew. Chem.* **2005**, *117*, 3734–3754; *Angew. Chem. Int. Ed*. **2005**, *44*, 3668–3688.
9. de Miranda, A.S.; Miranda, L.S.M.; de Souza, R.O.M.A. *Biotechnol. Adv.* **2015**, *33*, 372-393.
10. Bevinakatti, H.S.; Newadkar, R.V.; Bane, A.A. *J. Chem. Soc., Chem. Commun.* **1990**, 1090-1091.
11. Bodalo, A.; Gomez, J.L.; Gomez, E.; Bastida, J.; Leon, G.; Maximo, M.F.; Hidalgo, A.M.; Montiel, M.C. *Enzyme Microb. Tech.* **1999**, *24*, 381-387.
12. Brown, S., Parker, M.C., Turner, N. *Tetrahedron: Asymmetry* **2000**, *11*, 1687–1690.
13. Turner, N.; Winterman, J.; McCague, R.; Parratt, J.; Taylor, S. *Tetrahedron Lett.* **1995**, *36*, 1113-1116.
14. Podea, P.V.; Toşa, M.I.; Paizs, C.; Irimie, F.D. *Tetrahedron: Asymmetry* **2008**, *19*, 500–511.
15. Paizs, C.; Toşa, M.I.; Bencze, L.C.; Brem, J.; Irimie, F.D.; Rétey, J. *Heterocycles*, **2011**, *82*, 1217-1227.
16. Meerwein, H.; Buchner, E.; van Emster, K. *J. Prakt. Chem* **1939**, *152*, 237-266.

3. DISEMINAREA REZULTATELOR CERCETĂRII AFERENTE ETAPEI DIN ANUL 2015

În afara rezultatelor prezentate mai sus, datele obţinute în urma investigaţiilor experimentale originale proprii etapei derulate în anul 2015, precum şi în cadrul etapelor anterioare, au fost incluse în:

4 articole publicate/acceptate in reviste cotate ISI (factor de impact cumulat 5.656)

1. Dan Cascaval, Ramona Mihaela Matran, Marius Turnea, Anca-Irina Galaction, Alexandra Cristina Blaga, Distribution of mixing efficiency in a split-cylinder gas-lift bioreactor for *Yarrowia lipolytica* suspensions, *Canadian Journal of Chemical Engineering* 2015, 93(1), 18-28 (IF: 1.231).
2. László Csaba Bencze, Balázs Komjáti, Laura-Ancuta Pop, Csaba Paizs, Florin-Dan Irimie, József Nagy, László Poppe, Monica Ioana Tosa: Synthesis of enantiopure L-(5-phenylfuran-2yl)alanines by a sequential multienzyme process, *Tetrahedron: Asymmetry* **2015**, *26*, 1095–1101 (IF 2.155)
3. *Anca-Irina Galaction, Alexandra Cristina Blaga, Ramona Mihaela Matran, Dan Caşcaval,* Effect of bed configuration of immobilized biocatalysts on Penicillin G hydrolysis efficiency, *Korean Journal of Chemical Engineering* 2015, 32(2), 216-221 (IF: 1.166).
4. Ramona Mihaela Matran, Anca-Irina Galaction, Alexandra Cristina Blaga, Marius Turnea, Dan Cascaval, Distribution of Mixing Efficiency in a Split-Cylinder Gas- Lift Bioreactor with Immobilized Yarrowia lipolytica Cells Used for Olive Oil Mill Wastewater Treatment, *Chemical Engineering Communications* 2015 (IF: 1.104).

4 participări (postere) la manifestări ştiintifice internaţionale

1. Anca Irina Galaction, Lenuţa Kloetzer, Alexandra Cristina Blaga, Marius Turnea, Dan Caşcaval, New configuration of immobilized *A. succinogenes* bed for succinic acid production, *International Conference on Environment, Energy and Biotechnology (ICEEB 2015)*, Madrid, 15 - 16 Mai 2015.
2. Alexandra Cristina Blaga, Alexandra Tucaliuc, Corina Paraschiva Ciobanu, Anca-Irina Galaction, Marius Turnea, Dan Caşcaval, Distribution of mediated oxygen transfer rate in stirred bioreactors using oxygen-vectors, *19th Romanian International Conference on Chemistry and Chemical Engineering,* Sibiu, 2 - 5 Septembrie 2015
3. Anca-Irina Galaction, Marius Alexandru Turnea, Lenuta Kloetzer, Mădălina Poştaru, Dan Caşcaval, Anaerobic biodegradation of pyridine in a stationary basket bioreactor with immobilized *Bacillus spp.* cells, *8th International Conference on Environmental Engineering and Management*, Iaşi, 9 - 12 Septembrie 2015
4. Norbert-Artur Dima, Alina Filip, Monica Ioana Tosa, Csaba Paizs: *Pc*PAL's biocatalytic activity on benzofuran-2-yl-alanines, *IsySyCat (International Symposium on Synthesis and Catalysis)*, Evora, Portugalia, 2-4 sept. 2015

DEZVOLTAREA RESURSEI UMANE

- ABILITAREA directorului de proiect cu teza: BIOCATALYTIC APPROACHES FOR THE STEREOSELECTIVE SYNTHESIS OF CHIRAL BUILDING BLOCKS (OM Nr. 4920/18.08.2015)
- FINALIZAREA TEZEI DE DOCTORAT a unui membru al echipei de cercetare a proiectului, Ing. MARA ANA NAGHI: Lipase-mediated kinetic resolution towards enantiomerically enriched α- and β-hydroxy acids and their derivatives (OM Nr. 4643/30.07.2015)

Conf. Dr. Habil. MONICA IOANA TOSA

Prof. Dr. Ing. DAN CASCAVAL